Characterization Procedure for the Analysis of Arc Welding Fume

A comprehensive characterization procedure is described for the collection and analysis of ER70S-6 welding fume

BY J. W. SOWARDS, A. J. RAMIREZ, J. C. LIPPOLD, AND D. W. DICKINSON

ABSTRACT. A procedure has been developed to characterize welding fume generated from arc welding processes that includes the measurement of fume generation rate (FGR), fume particle size, and mass distribution, and the morphology, chemistry, and composition of the fume. Fume was collected using both a state-of-the-art collection chamber and an electrical low-pressure impactor (ELPI), the former designed to optimize fume collection and the latter allowing fume to be segregated into 12 size ranges from 0.03 to 10 μm. Detailed characterization of fume particles was conducted using a combination of x-ray diffraction (XRD), transmission electron microscopy (TEM), scanning electron microscopy (SEM), x-ray energy dispersive spectroscopy (XEDS), and x-ray photoelectron spectroscopy (XPS). These techniques, when used collectively, provide extensive information on welding fume particle structure, composition, and morphology. Using the ELPI, composition and morphology can be studied as a function of particle size. In this paper, the collection and analysis procedure is described in detail, and an example analysis of the ER70S-6 welding wire is provided. Welding fume characterization methods were performed on fume generated by gas metal arc welding (GMAW) of the ER70S-6 welding wire with 100% CO_2 and 75%Ar-25%CO_2 shielding gases. The combined techniques provide a comprehensive understanding of the fume generated by arc welding consumables.

Introduction

Fume generated by arc welding processes is an unfortunate byproduct and general nuisance to the welding industry. The principal concern with welding fume is associated with health risks resulting from fume inhalation. Additionally, government regulations continue to decrease the exposure limits to the various elements that are contained in the fume (Ref. 1). Several studies have examined welding fume generated from a variety of processes and consumables in an attempt to better understand the different aspects of fume behavior. These include fume generation studies (Refs. 1–6) as well as several characterization studies (Refs. 7–10), which used a variety of characterization techniques such as XRD, SEM, and TEM.

These and some other advanced techniques have been combined in this study to obtain a more comprehensive insight on composition and morphology of welding fume relative to both the bulk fume as well as individual fume particle chemistry and morphology. The use of an aerosol cascade impactor to separate fume into different size ranges allows fume to be studied as a function of particle size. This is a particularly important part of this approach since fume inhalation is affected by its size and aerosol characteristics.

Jenkins et al. have provided a summary of techniques that can be used for fume analysis (Ref. 11). Their synopsis showed that reporting molar concentration of elements on the fume is more adequate than reporting atomic percentage and makes it easier to compare results from different techniques as SEM-XEDS, TEM-XEDS, and XPS. X-ray photoelectron spectroscopy is a surface analytical technique that allows the measurement of fume-born particle surface composition and has been used in previous fumes studies (Refs. 8, 9, 11–13). Since this technique is surface sensitive, it is ideal for analyzing the exterior layers of fume particles, which are most likely first to interact in the body after ingestion or inhalation. XRD analysis, which has become a fairly standard practice to analyze bulk fume, is a good technique for determining crystallographic structure of fume particles. This technique is normally used to analyze bulk fume samples and is very effective for determining the major metallic species and compounds that are present. On the other hand, electron microscopy allows individual particle characterization.

This paper outlines a procedure (Fig. 1) for collection and analysis of bulk welding fume samples and analyzing compositions of individual size ranges provided by an electrical low-pressure impactor (ELPI) made by Dekati Ltd. of Finland. Using this procedure, the fume produced by the GMAW process using ER70S-6 welding wire is analyzed, and the results of the various analytical techniques are presented. Fume from this consumable in size ranges including the ultrafine (0.03–0.1 μm), fine (0.1–2.5 μm), and coarse (2.5–10 μm) particle sizes were collected and analyzed with the analytical techniques described previously.

KEYWORDS

Fume Generation Rate
Fume Particle Size
ER70S-6 wire
Gas Metal Arc Welding
Shielding Gases
Welding Fume

J. W. SOWARDS (sowards.18@osu.edu), *J. C. LIPPOLD, and D. W. DICKINSON are with the Welding & Joining Metallurgy Group, The Ohio State University, Columbus, Ohio. A. J. RAMIREZ is with the Brazilian Synchrotron Light Laboratory, Campinas, SP, Brazil.*

Fume Collection Procedures

Welding Procedures

The welding wire used for this study was ER70S-6 and base material was A-36 steel. The compositions of welding wire, base material, and weld deposits produced with two different shielding gases are shown in Table 1. The short circuit transfer mode was used for welding with both gases, and nominal welding parameters were developed that represented a mid-range heat input (according to the manufacturer's recommended operating range) level for this filler metal. The welding power supply was a Miller constant current square wave machine that outputs 300 A/32 V at 60% duty cycle. Welding parameters are presented in Table 2. Test welds for fume generation rates were performed on 8-in. (20.3-cm) square A36

plates in circular paths around the base plates. Plate motion was achieved via a rotary positioning system within the fume enclosure during these tests. The GMAW gun was inserted through the back of the enclosure and contact tip to work distance was adjusted by a vertically mounted linear positioning system. Welds for ELPI collections were performed on 4- × 12-in. (100- × 300-mm) plates with a stationary torch position and base metal motion via linear positioner. Process variables (current, voltage, weld time) were obtained using a data acquisition system manufactured by Weld QC, Inc.

Fume Chamber

The American Welding Society Specification F1.2:1999, *Laboratory Method for Measuring Fume Generation Rates (FGR) and Total Fume Emission of Welding and Allied Processes*, describes the construction and use of a fume collection enclosure (Ref. 14). This chamber design, shown in Fig. 2A, was modified from the AWS designation to incorporate smaller filter pore sizes ensuring collection of the smaller particle size ranges by using a 0.3-µm pore size filter instead of the recommended 4-µm filter. The conventional air pump was replaced by a high-volume air sampler system with a built-in flow adjuster assembly built specifically for air sampling systems by the Staplex Co. of Brooklyn, N.Y. The filters, also made by Staplex, are 8- ×10-in. (200- ×250-mm) glass fiber filters with a 0.3-µm pore size and collection efficiency of 99.98%. The flow rate may be varied and monitored from 0 to 70 ft^3/min (2000 L/min), double that of the maximum specified by AWS; pressure drop across the filter was measured via a digital manometer with computer data acquisition capabilities.

For FGR measurements, the air pump flow rates on the fume hood are initially set to approximately 25 ft^3/min (700 L/min). Flow rate decreases as fume particulate starts to obstruct the filter pores. As indicated in Fig. 3, Region I corresponds to airflow through the clean filter, Region II is where the collection occurs and the pressure drop increases as particles congest the filter pores, and Region III shows that filter saturation has been reached and no additional fume may be deposited onto the filter. Tests are normally stopped before saturation is reached to allow all fumes to clear the chamber and be deposited on the filter paper. A regression fit for the pressure drop across the filter showed an increase proportional to t^2, the collection time, as shown in the inset of Fig. 3. Filters were tested for comparison to the flow rate and pressure drop recommended by the AWS test. The initial results indicated that the smaller filter pores have better particle retention due to the increase in pressure drop for flow rates that correspond to the AWS-type test. The fume generation rates (FGRs) were measured in triplicate for ER70S-6 with both shielding gases as displayed in Fig. 4 along with some FGRs from other consumables tested with this method as a comparison. Standard deviation of the measurements is shown with error bars. Particles collected from welds produced with the two different shielding gases have quite similar composition since the welding wire is the same, though previous studies have shown differences in FGR values for different shielding gases (Refs. 5, 15, 16).

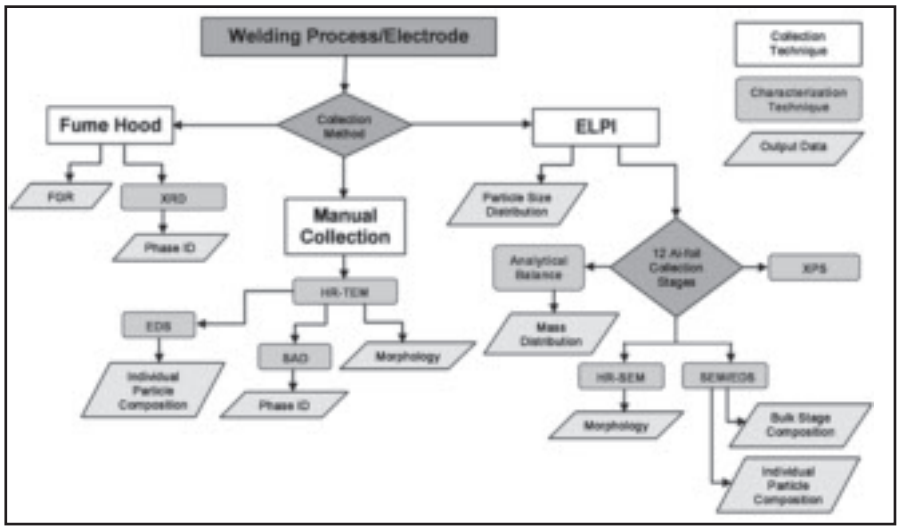

Fig. 1 — Flow chart outlining collection and characterization procedure.

Electrical Low-Pressure Impactor

Aerosol collection techniques including scanning mobility particle sizing (SMPS) (Ref. 6) and low-pressure cascade impaction (Ref. 9) have been used in the past to collect welding fume and report size distribution information. Collection in the present study was performed with an ELPI, which was designed for real-time monitoring of aerosol particle size distributions. Using 12 detection channels, the ELPI has the ability to distinguish a size distribution range of 0.03 to 10 µm by sensing electrical currents of charged particles. The operating principle is based on charging, particle inertia, and electrical

Table 1 — Composition (wt-%) of Wire, Base Plate, and Weld Deposits (Measured Using Mass Spectrometry and LECO® technique)

Element	ER70S-6 Wire	A36 plate	100% CO_2 Deposit	75% Ar-25% CO_2 Deposit
C	0.063	0.18	0.12	0.11
Mn	1.54	0.70	1.00	1.13
Si	0.90	0.19	0.47	0.63
P	0.009	0.012	0.009	0.010
S	0.007	0.020	0.015	0.013
Ni	0.011	0.10	0.045	0.042
Cr	0.011	0.064	0.031	0.030
Mo	0.002	0.022	0.014	0.013
Cu	0.12	—	0.020	0.018

Table 2 — Welding Conditions Used for Generation of Welding Fume from ER70S-6 Wire

Welding Parameter	100% CO_2	75% Ar-25% CO_2
Current, amps	158	164
Voltage, volts	20.4	18.1
Wire Feed Speed, in./min (mm/s)	169 (72)	168 (71)
Travel Speed, in./min (mm/s)	10.5 (4.5)	10.5 (4.5)
Calculated Heat Input, kJ/in. (kJ/mm)	18.5 (0.73)	17.00 (0.67)

Electrode diameter = 0.045 in. (1.14 mm), gas flow rate = 30 ft^3/h (14.2 L/min), contact tip to work distance = 0.5 in. (12.7 mm), gas nozzle to work distance = 0.5 in. (12.7 mm)

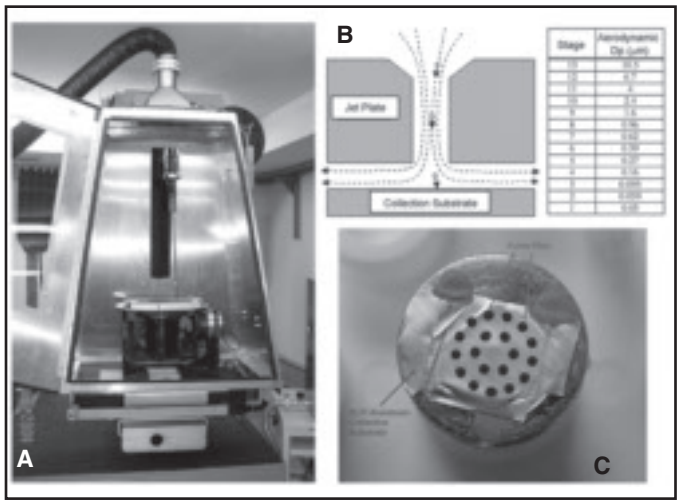

Fig. 2 — A — Fume collection hood, electrode feed system, and rotary positioning system; B — schematic of cascade impactor operation and average particle diameters for each stage; C — aluminum collection substrate from the ELPI mounted on an aluminum SEM analysis post. The fume particle piles are clearly evident as the dark spots on the substrate.

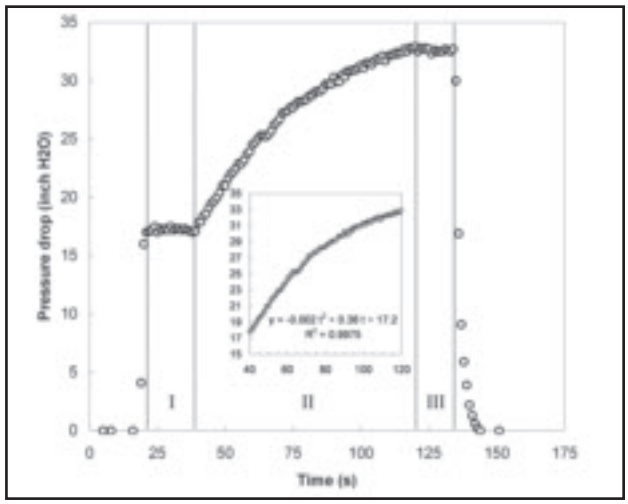

Fig. 3 — Pressure drop vs. time for 0.3 μm glass fiber filter during fume collection.

detection (Ref. 17). Fume is gathered at a location near the source of fume generation then drawn toward the ELPI through Tygon® tubing with vacuum. The fume passes through a corona charger after entering the ELPI, which produces a field of ions and places a positive charge on the incoming fume particles. Once charged, the particles enter the impactor column where they are separated by inertial classification according to aerodynamic diameter as they pass through the different stages. As the fume passes through the jet plate of each successive stage, particles larger than a certain dimension are unable to make the sharp turn required to reach the following stage, causing them to impact on the collection substrate directly below the preceding stage as illustrated in Fig. 2B. Each stage has a particular cutoff diameter that determines the particle size that should not pass through to the following stage. This diameter is defined as the aerodynamic diameter of particles collected on that stage with an efficiency of 50% (see Fig. 2). Aluminum foil substrates were used for collection since they provide a highly conductive surface for electron microscopy. For determining mass and size distributions, these substrates were coated with a thin layer of Si grease before collection was performed so that particle "bounce" was eliminated, thereby enhancing particle sticking on the substrate. Fume was drawn through the system by means of low vacuum pressure created by an external vacuum pump.

After particles impact with each collection stage, their charge was detected by current-sensing electrometers. This current data is used to develop the number distributions as seen in Fig. 5. These distributions are an average of three measurements collected with the ELPI with error bars indicating one standard deviation (valid for percentage scale only) of the three measurements. The distributions for the ER70S-6 electrode show little variation with changes in shielding gas for the coarse particle size range (>2.5 μm). Distributions begin to diverge in the lower end of the fine particle range as the 75/25 is skewed toward larger particle sizes in this range. The 100% CO_2 gas has an increase in particle concentration in the low detection range of the ELPI (30 nanometers). Statistical analysis may be performed on these distributions to find geometric mean diameter and geometric standard deviation. The results of these calculations are summarized in Table 3 for the size and mass distributions.

A possible reason for variations in particle size distribution among the different shielding gases is a difference in oxidation potential between particles in the different gas types leading to slight composition changes after particle nucleation (Ref. 18). Particle density changes with oxidation potential, e.g., the Ar gas hinders particle oxidation resulting in higher concentrations of Fe-rich particles as opposed to

Table 3 — Statistical Analysis of Size Distributions Including Mean Diameter, Standard Deviation, and Ranges of Particle Sizes within which Lie 67% and 95% of All Particles

Shielding Gas	Geometric mean diameter (μm)	Calculated[a] geometric mean diameter (μm)	Geometric standard deviation (μm)	67% range (μm)	95% range (μm)
Number Distribution Statistics					
100% CO_2	0.049		2.06	0.024–0.103	0.012–0.206
75% Ar-25% CO_2	0.058		2.10	0.027–0.121	0.014–0.243
Mass Distribution Statistics					
100% CO_2	0.386	0.305	2.99	0.129–1.156	0.064–2.313
75% Ar-25% CO_2	0.338	0.398	2.71	0.125–0.916	0.062–1.833

(a) The geometric mean diameter of the mass distribution was calculated from the geometric mean diameter of the number distribution with the Hatch-Choate equation (Ref. 20).

Fe-oxide, which has a lower density. The slight density increase causes the distribution to shift to higher aerodynamic diameters. The definition of aerodynamic diameter, a principle the ELPI uses to separate particles, is that a diameter of a unit density sphere (1 g/cm^3) will have the same aerodynamic properties as a particle of interest (Refs. 17, 19). Therefore, a dense Fe-rich particle with the same diameter of an Fe-oxide particle will settle on a higher stage of the impactor causing the distribution shift toward higher aerodynamic diameters. In addition to the effect of the shielding gas on the particles' density and, consequently, on the size distribution, the difference in the oxidation potential of the gas will have important influence on fume particle formation.

Mass distributions were obtained by weighing the collection substrate of each stage prior to and after the collection with a precision analytical balance accurate to 10^{-5} g. The mass distributions that were measured may be plotted as shown in Fig. 6 vs. the particle diameter. This allows for a comparison between the number of particles and the particle mass of each size. Error is indicated for an average of three measurements, again showing one standard deviation of error (valid for percentage scale only). The mass distributions peak at approximately 0.25 μm aerodynamic diameter. Discrepancies between the size and mass distributions can be explained by the fact that particles on the smaller stages, while much larger in number than the center stages, have a much smaller mass. Individual particles on the top stages have the highest mass but are the fewest in number. The mass distribution for 100% CO_2 shielding gas is shifted to slightly higher particle sizes.

The Hatch-Choate equation (Ref. 20) was used to convert the geometric mean diameter of the number distribution to that of the mass distribution to evaluate the performance of the ELPI functioning as an electrometer. The calculated (with Hatch-Choate equation) geometric mean mass diameter is included in Table 3. Relative error (%) between the measured and calculated mean mass diameters for the 100% CO_2 and 75% Ar-25% CO_2 shielding gases were approximately 21 and 18%, respectively. These values indicate the correlation between the ELPI's ability to measure number distribution (electronically) vs. the mass distribution obtained by weighing ELPI stages. Note that some error may arise from the conversion itself since Hatch-Choate assumes "perfect" log-normal distributions.

Analytical Characterization

Characterizing individual and bulk welding fume particles is highly important to understand the fumes' formation phenomenon and the possible impact of fume on the health of those working in metal joining areas. Fumes are an undesirable byproduct of the various arc welding processes and have motivated many studies over the past 50 years as speculation has increased of medical problems arising from overexposure to fume during welding. It is important to consider each of these size ranges independently from one another since they are generally formed by different mechanisms. The following techniques are ideal for analyzing different characteristics of fume such as structure, morphology, and composition.

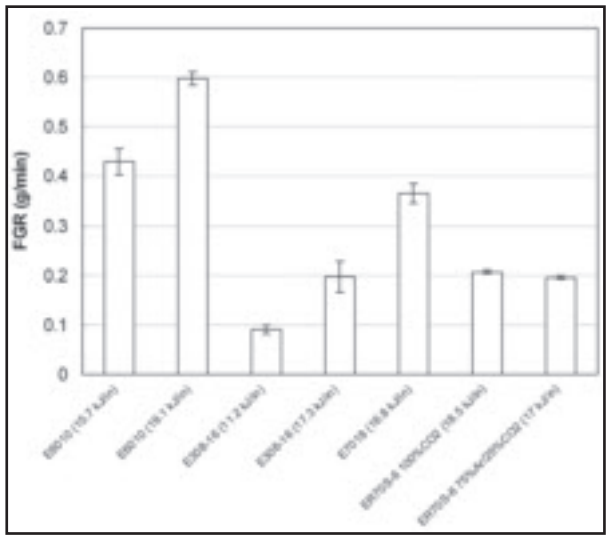

Fig. 4 — FGR values for several electrodes tested with the fume collection hood and high-efficiency 0.3-μm glass fiber filter.

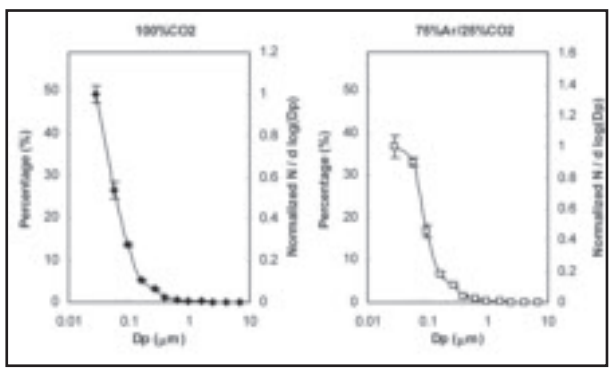

Fig. 5 — Particle size distribution measured with ELPI, where D_p is particle aerodynamic diameter. Error bars indicate one standard deviation of three collections for the percentage scale.

X-Ray Diffraction

X-ray diffraction experiments were performed on fume collected on the bulk fume filters from the fume hood to obtain information on the phases present in welding fume. This technique is a good starting

Table 4 — Bulk ELPI Stage Compositions as Measured with XEDS

	wt-% ER70S-6 100% CO_2				wt-% ER70S-6 75% Ar/25% CO_2			
Element	Stage 2	Stage 4	Stage 8	Stage 10	Stage 2	Stage 4	Stage 8	Stage 10
SiK	6.6	10.1	4.3	2.1	9.5	10.1	6.3	3.5
MnK	11	13.2	13.8	7.7	10.7	11.7	10.9	6.4
FeK	80.9	76.2	81.9	87.2	78.3	78.2	82.3	90.1
CuK	1.5	0.4	0	3	1.5	0	0.4	0
	at.-% ER70S-6 100% CO_2				at.-% ER70S-6 75% Ar/25% CO_2			
Element	Stage 2	Stage 4	Stage 8	Stage 10	Stage 2	Stage 4	Stage 8	Stage 10
SiK	12.4	18.2	8.2	4.1	17.3	18.2	11.8	6.7
MnK	10.5	12.2	13.4	7.7	9.9	10.8	10.4	6.3
FeK	75.9	69.2	78.4	85.6	71.6	71	77.4	87
CuK	1.2	0.4	0	2.6	1.2	0	0.4	0
Dp (μm)	0.059	0.16	0.96	2.4	0.059	0.16	0.96	2.4

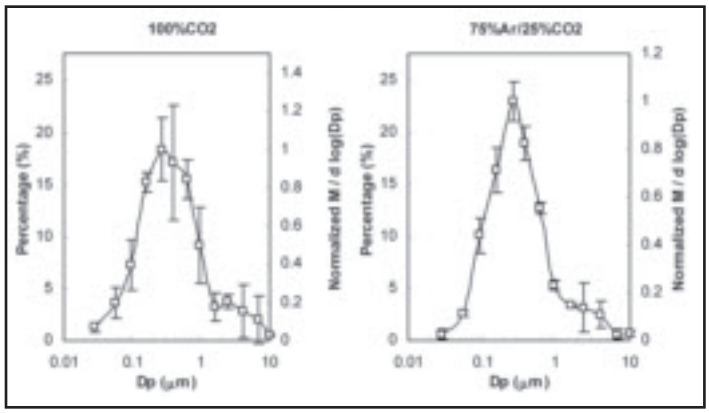

Fig. 6 — Particle mass distribution collected with ELPI. Masses were measured with precision analytical balance, where D_p is particle aerodynamic diameter. Error bars indicate one standard deviation of three collections for the percentage scale.

Table 5 — Chemical Composition of Fume Particles Shown in Fig. 9 as Measured with SEM–XEDS (Composition Is Reported in Atomic-Percent)

Element	XEDS Spot Analysis (at.-%)			
	1	2	3	4
Si K	1.4	1.5	17.5	23.7
Mn K	0.5	0.5	9.4	13.1
Fe K	97.3	97.3	73.1	62.9
Cu K	0.7	0.6	0.0	0.3

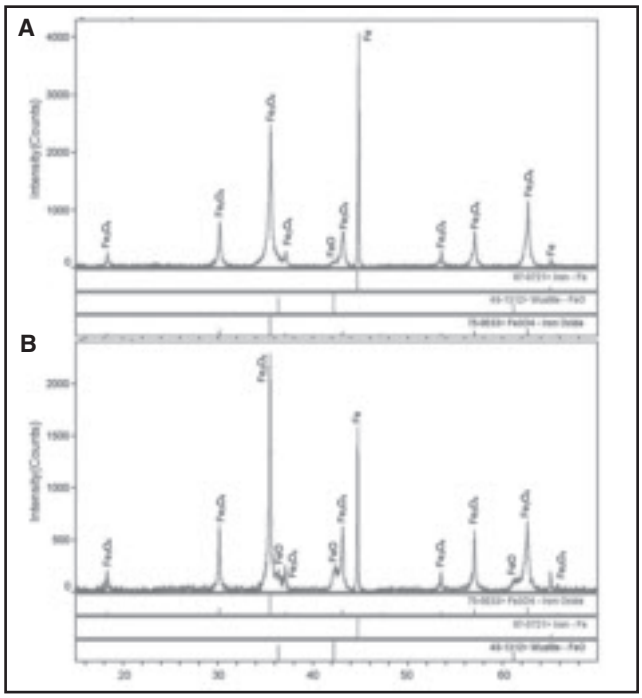

Fig. 7 — XRD spectrum of bulk fume produced from ER70S-6 fume with the following: A — 75% Ar-25% CO_2 shielding gas; B — 100% CO_2 shielding gas.

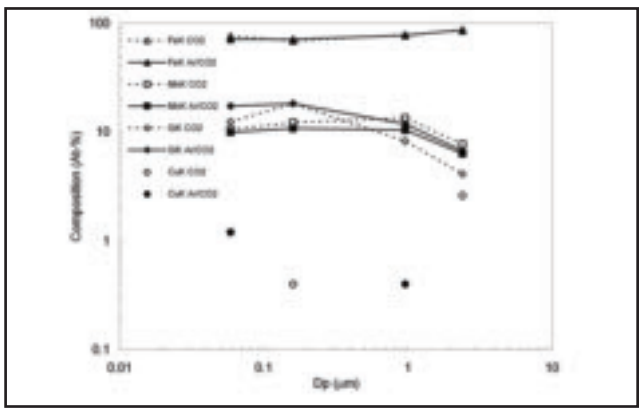

Fig. 8 — Distribution of bulk fume composition vs. particle diameter for both shielding gases as measured with SEM-XEDS on ELPI stages. Note that oxygen was present on each stage but was not quantified.

point for the analysis techniques to follow because it provides basic phase identification. In addition, much of the previous analysis work on welding fume has included XRD of bulk fume samples, which makes a nice point of reference with respect to comparisons of structure and phase information found in previous studies.

Fume from the FGR tests was transferred onto off-axis zero background Si-crystal sample slides after a thin coating of petroleum jelly was applied to the slide to allow the fume to adhere. Data were collected using a Scintag XDS-2000 diffractometer equipped with a Cu x-ray tube and an energy-dispersive i-Ge detector. The goniometer was a vertical θ-θ arrangement in a standard Bragg-Brentano geometry. Data analysis was performed using MDI Jade software (version 6.1) and Bruker/Socabim EVA (version 7.0). The phases were identified by comparison with the ICDD/ICSD 2002 PDF database.

Figure 7 shows the diffraction patterns of fume obtained from 100% CO_2 and 75% Ar/25% CO_2 shielding gases with heat inputs of 18.4 and 16.8 kJ/in. (0.72 and 0.66 kJ/mm), respectively. Intensity of each phase is plotted on the y-axis and the Bragg angle is plotted on the x-axis. Two phases identified in fume from both gas types were Fe_3O_4 (magnetite) and Fe. An additional phase, FeO (wustite), was found in the fume from 100% CO_2 shielding gas. Oxidation potential is higher in this case resulting in the additional oxide. Since the oxidation potential of the 75% Ar/25% CO_2 gas is lower, more metallic Fe is seen in that case as opposed to the 100% CO_2 shielding gas. These samples were collected with the bulk fume collection hood, thus the phases represent the entire size range of welding fume particulate generated for both conditions.

Scanning Electron Microscopy

Scanning electron microscopy and x-ray energy dispersive spectrometry are ideal for examining particle morphology and measuring bulk and individual particle compositions, respectively. The SEM is the most efficient method to determine both the composition and morphology of the large- and medium-size particles from the individual stages collected in the ELPI since little sample preparation is required and many analyses can be completed in a relatively short time. Average composition of fume particles on each stage can also be determined by analyzing the small piles of fume that form on the aluminum substrate during fume collection in the ELPI (see Fig. 2C). These piles consist of many particles and, thus, this type of analysis represents an average of many fume particles. In addition, individual fume particles may be analyzed and the composition of particles of different sizes compared. A limitation of the SEM is that equipment does not allow the composition of particles below approximately 0.3 μm in diameter to be easily analyzed since the electron beam interacts with a volume of at least this size, depending on the accelerating voltage.

Bulk composition of fume particles from Stages 2, 4, 8, and 10 of the ELPI were analyzed representing average fume particle sizes of 0.06, 0.16, 0.96, and 2.4 microns, respectively. Only fume particles collected on aluminum collection plates in

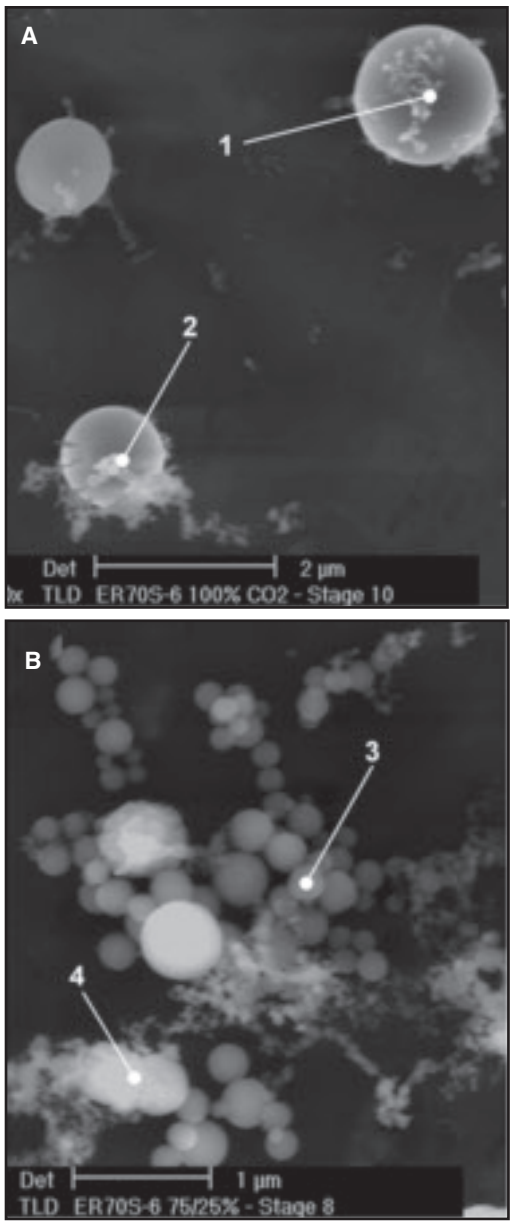

Fig. 9 — Secondary electron SEM micrographs of fume generated from ER70S-6 wire with the following: A — 100% CO_2; B — 75% Ar-25% CO_2.

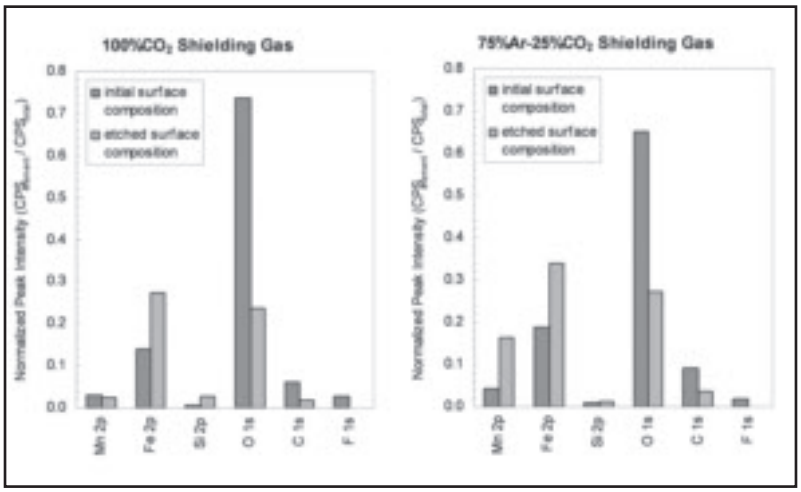

Fig. 10 — XPS peak intensities as a function of etching for two shielding gases.

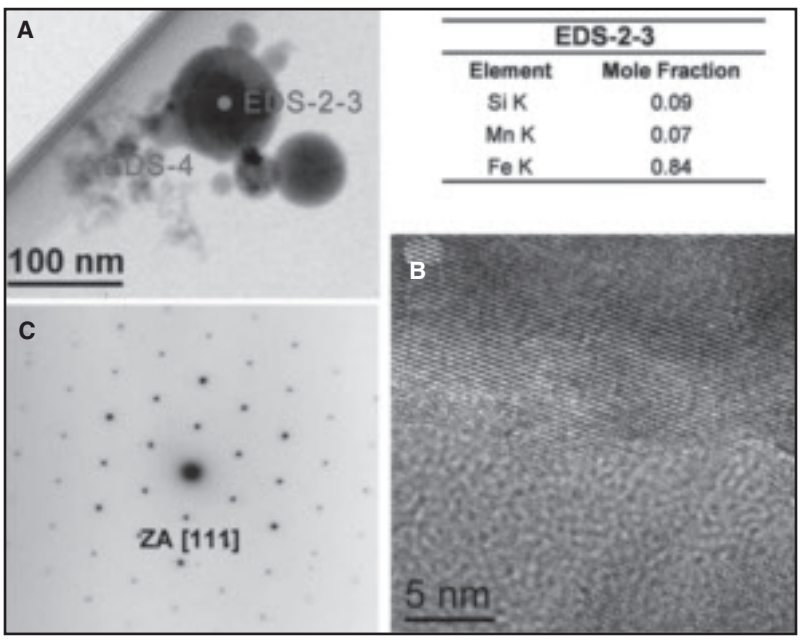

Fig. 11 — Spherical particle from ER70S-6 (100% CO_2) fume. TEM micrographs: A — Normal; B — high-resolution; C — SAD pattern on [111] zone axis of particle identifying $(Mn,Fe)_3O_4$.

the ELPI were analyzed. Figure 2C is an example of an aluminum collection plate mounted on an aluminum SEM analysis post. The center region of a given fume pile (roughly 100 µm in diameter) represents the region where the average compositions of the fume particles for each stage were determined. A summary of the average compositions in both weight-percent and atomic-percent for the four stages analyzed are provided in Table 4 and Fig. 8. The data show that Mn is present in uniform concentrations on each stage. The amount of Fe for any given stage appears to be dependent on the amount of O present on that stage since an Fe increase is generally accompanied by a decrease in O and vice versa. Fe also increases in concentration with increasing particle size. Cu (from the wire coating) concentration appears to increase and Si decreases as particle size increases in 100% CO_2 shielding gas. Cu decreases with particle size for the 75% Ar-25% CO_2 mixture. Na and S were present in trace amounts in the bulk composition analysis.

Chemical analysis was performed on individual particles using an electron beam spot (rather than rastering) on a given particle of interest. Monte Carlo simulations performed with Casino (Ref. 21) showed the interaction volume of the beam with the particle generates x-rays from the entire volume of the particle thus providing an average composition. The chemical analyses were performed for approximately 15 particles on each stage of the ELPI including spherical, agglomerated, and irregular particle morphologies. An example of several spot XEDS analysis locations and corresponding compositions are shown in Fig. 9 and Table 5, respectively. Note that XEDS measurement locations 3 and 4 are an average of several of the surrounding particles since particle size is less than electron beam interaction volume. The compositions measured from individual particle analyses generally coin-

cided with the bulk composition of that stage, thus bulk analyses were good indications of individual particle composition with respect to particle diameter.

Particle morphology of each ELPI stage may also be examined with the SEM since there is a broad magnification range allowing for imaging of particles on every stage. Micrographs were examined to determine the morphologies of each stage. These include three different types of particles. Agglomerated particles are the most frequent on each stage. These are generally found as large groupings of spherical particles an example of which is shown in the micrograph of Fig. 9B. Isolated spherical particles are also common though present in a much lower frequency. Irregular-shaped particles have also been observed but are present in the lowest frequency of the three particle morphologies. Particle morphology is important to consider since it determines the surface area of a particle and the particles aerodynamic diameter. An agglomerate has a much larger surface area than an individual spherical particle with the same cross section. These agglomerates also have different aerodynamic properties that may affect the degree to which they can be inhaled.

X-Ray Photoelectron Spectroscopy

X-ray photoelectron spectroscopy (XPS) is a surface-sensitive chemical analysis technique that is used to obtain information on the oxidation state for the elements in welding fume. Normal sampling depth is on the order of several angstroms (Ref. 22). Previous studies have incorporated surface-sensitive techniques into welding fume studies (Refs. 8, 9, 11–13, 23) because particle interaction with human tissues most likely occurs with the surface of particles, thus surface chemistry is possibly the most important aspect when considering chemistry.

XPS uses "soft" x-ray radiation to bombard a sample (Ref. 24). Unlike XRD, where the x-ray is diffracted by the crystal lattice, in XPS the x-ray is absorbed and a photoelectron is ejected. By subtracting the energy of the impinging x-ray (which is known) and the energy of the electron (which is measured), the binding energy of the electron can be determined. Based on this information, the composition and valence states of various elements can be determined. Most instruments are equipped with a "sputtering" gun that bombards the surface with argon atoms, thereby removing layers of atoms from the surface revealing the composition of the underlying material. This depth profiling feature of XPS allows both the surface and underlying compositions of fume particles to be examined and the valence states of various metallic elements to be determined.

The XPS system used for this study was a Kratos Ultra Axis XPS and UPS system with depth profiling capabilities using Ar^+ ion etching. XPS analysis for both shielding gas types was performed using fume collected on Stage 3 of the ELPI that has an average particle diameter of 0.095 microns.

XPS shows that the outer surface of the fume particles is highly oxidized and is consistent with the Fe_3O_4 and FeO compounds found in XRD. Etching of the fume particles results in a reduction of the oxygen concentration and an increase in the presence of metallic species. The peak intensity measured for each peak in counts per second (CPS) were normalized to the total intensity and plotted as shown in Fig. 10. Both metallic Fe and Mn peaks were present after etching, in addition to oxides containing both Fe and Mn. The degree of surface oxidation was greater with the 100% CO_2 shielding gas relative to the 75% Ar-25% CO_2 shielding gas. Copper was also detected in low levels, but only after etching of the particles. Based on combined XRD and XPS data, the valence state of iron and manganese appears to be $(Fe,Mn)^{+2}$ and $(Fe,Mn)^{+3}$ in fumes from both shielding gases.

Transmission Electron Microscopy

Transmission electron microscopy (TEM) provides the highest spatial resolution available for determining both the morphology and composition of individual fume particles less than approximately 300 nanometers in diameter. This technique is commonly used to analyze several types of aerosols since it can image nanoscale particles better than other methods providing insight into morphology, crystallographic and electronic structures, and chemical composition of the ultrafine particle sizes (Ref. 22). Scanning transmission electron microscopy has been used in the past to characterize welding fume morphology and composition (Refs. 9, 10).

The TEM analyses were performed with a JEOL HRTEM JEM 3010 coupled with chemical micro- and nano-analysis by XEDS system equipped with a Si(Li) detector. A double-tilt beryllium sample holder was used for crystallographic analysis and low background chemical analysis. TEM analysis was performed at 300 kV using a wide range of magnifications, from 10,000 to 1,000,000 ×. Several techniques, including bright field, dark field, selected area diffraction, nano-beam diffraction, and XEDS microanalysis were also performed. Microanalysis probes of 5- and 25-nm diameters were used along with 400-s spectra collection times to provide adequate counting statistics. Images and electron diffraction patterns were recorded on TEM film as well as digitally using a 1024 × 1024 pixel CCD camera.

Samples were directly collected at 3 in. above the arc by passing carbon-coated gold TEM grids through the fume plume. Additional samples were collected in Stages 1–4 of the ELPI as a comparison. As revealed by the SEM analysis, the ELPI stages contained a mixture of individual fume particles and agglomerates. Both direct collections above the welding arc and in the ELPI revealed the presence of individual and agglomerated particles, which agrees with previous findings that fume particle agglomeration occurs within the vicinity of the arc. This is of little surprise since particles begin to collide with one another almost immediately after they nucleate into a vapor. While some additional agglomeration may occur within the ELPI, it does not appear to be significant.

Detailed TEM analysis was conducted on fume particles that were captured on TEM grids held just above the welding arc, using procedures described previously. Fume from ER70S-6 welds made with both 100% CO_2 and 75% Ar/25% CO_2 were analyzed, but no significant, or systematic, difference between the fume generated using these shielding gases could be determined. Two general types of particles were analyzed. The first type was individual spherical particles in the range from 20 to 100 nm (0.02–0.1 μm). Most of these particles exhibited a core-shell structure with the core consisting of an Fe_3O_4 or $(Fe,Mn)_3O_4$ structure, surrounded by a Si-rich shell. The second type was an agglomerate morphology consisting of many very small spherical particles, typically in the range from 10 to 20 nm (0.01 to 0.02 μm). Many of these particles were of the $(Fe,Mn)_3O_4$ type and also exhibited a core-shell structure with a Si-rich shell. Other particle types such as Fe- and FeO-rich particles detected using XRD analysis were not observed in the TEM analysis. Fe and FeO particles are likely much larger in size than those examined in TEM since they are formed from weld spatter, which cannot oxidize as heavily throughout the volume of the particles. A typical arrangement of TEM particle analysis micrographs are shown in Fig. 11 where A shows an agglomerate of nanoscale particles, B shows a high-resolution image of one of the particle shells, and C illustrates the resulting diffraction pattern of the pointed particle, which was identified as $(Mn,Fe)_3O_4$-type diffraction along the [111] zone axis.

Core-Shell Particle Structure

TEM revealed that the core-shell particle structure was common among the particles less than 100 nm in diameter. Contrary to this, the XPS analysis of similar particle

sizes did not reveal this trend since the Si 2p signal varied little as a function of particle etching depth (see Fig. 10). XPS is a surface-sensitive technique with a very limited spatial resolution. On the other hand, TEM is a technique that provides volumetric information of very small (thin) samples and has an outstanding spatial resolution. However, this outstanding spatial resolution may compromise the statistics of the results, especially if the analysis is performed by an inexperienced user and if it is not complemented with other techniques. In addition, the Ar-ion milling is not a very well-controlled process, especially on a heterogeneous surface such as the type tested. While using HRTEM it is possible to unequivocally identify a core-shell structure, it is a more complex matter using XPS especially in complex structures such as piles of sphere-like particles with a wide range of sizes, structures, and compositions. The information provided by HRTEM and XPS analyses is not expected to be identical but complementary; therefore, these techniques should be analyzed together and kept in context to avoid misinterpretation.

Conclusions

A combination of analytical techniques was used to examine welding fume generated from ER70S-6 wire with two different shielding gases (100% CO_2 and 75% Ar-25% CO_2). Fume was collected with an electronic low-pressure impactor (ELPI) that was used to find welding fume particle size and mass distribution in sizes ranging from 30 nm to 10 μm in size, and collect fume samples for further characterization studies. This instrument is very useful for the study of welding fume since it has the ability to separate particles into different size ranges and deposit them on substrates that may be evaluated individually by SEM, TEM, and XPS. Using this technique, the composition of welding fume was measured as a function of aerodynamic diameter. The results may be used to provide a comparison of respirable and irrespirable particles vs. their compositions.

Experimental results from XRD showed higher oxidation in the particles from fume generated with 100% CO_2 shielding gas compared with the 75% Ar-25% CO_2, which most likely results in a change in density of fume particles by shifting the ratio of oxygen and iron in the particles. The more heavily oxidized particles form smaller aerodynamic sizes on average than those with less oxidation, which is shown by the ELPI size distributions and statistical analysis of the 100% CO_2 gas vs. the 75% Ar-25% CO_2 mixture. TEM and XPS revealed higher oxygen content in particles from the 100% CO_2 shielding gas, which confirms why the shift is occurring.

Electron microscopy techniques permitted micro- and nano-analyses of the morphology, chemical composition, and crystallographic structure of agglomerates of particles and isolated particles. In the case of TEM, the analyses made possible the identification of core-shell structures in some of the particles.

This combination of characterization techniques has been employed to collect fume generated by GMAW, and to characterize the fume by size distribution, chemical composition, structure, and morphology, which requires the use of multiple imaging and analytical techniques since the size variation of welding fume particles is quite large.

Acknowledgments

The authors would like to thank Matt Gonser of the Welding & Joining Metallurgy Group at The Ohio State University for his valuable assistance in fume collection and analysis. Also thanks to Troy Paskell of WeldQC for help with equipment setup and testing. Funding for this project was provided by D&L Welding Fume Analysis LLC representing a consortium of past and current consumables manufacturers.

References

1. Castner, H. R., and Null, C. L. 1998. Chromium, nickel and manganese in shipyard welding fumes. *Welding Journal* 77(6): 223-s to 231-s.

2. *Fumes and Gases in the Welding Environment.* 1979. Miami, Fla.: American Welding Society.

3. Castner, H. R. 1995. Gas metal arc welding fume generation using pulsed current. *Welding Journal* 74(2): 59-s to 68-s.

4. Heile, R. F., and Hill, D. C. 1975. Particulate fume generation in arc welding processes. *Welding Journal* 54(7): 201-s to 210-s.

5. Zimmer, A. T., Baron, P., and Biswas, P. 2002. The influence of operating parameters on number-weighted aerosol size distribution generated from a gas metal arc welding process. *Journal of Aerosol Science* 33: 519–531.

6. Zimmer, A. T., and Biswas, P. 2001. Characterization of the aerosols resulting from arc welding operations. *Journal of Aerosol Science* 32: 993–1008.

7. *Characterization of Arc Welding Fume.* 1983. Miami, Fla.: American Welding Society.

8. Voitkevich, V. 1995. *Welding Fumes: Formation, Properties, and Biological Effects.* Cambridge, England: Abington Publishing.

9. Jenkins, N. T. 2003. *Chemistry of Airborne Particles from Metallurgical Processing.* PhD dissertation: Materials Science and Engineering, Massachusetts Institute of Technology, Cambridge, Mass.

10. Maynard, A. D., Yasuo, I., Arslan, I., Zimmer, A. T., Browning, N., and Nicholls, A. 2004. Examining elemental surface enrichment in ultrafine aerosol particles using analytical scanning transmission electron microscopy. *Journal of Aerosol Science and Technology.* 38: 365–381.

11. Jenkins, N. T., and Eagar, T. W. 2005. Chemical analysis of welding fume particles. *Welding Journal* 84(6): 87-s to 93-s.

12. Voitkevich, V. G. 1988. Etude, par spectroscopie photoelectronique a rayons X, de l'heterogeneite de la soudage (Investigation of heterogeneity of welding fume particle composition by the method of X-ray photoelectron spectroscopy). *Welding in the World, Le Soudage Dans Le Monde* 26: 108–111.

13. Tandon, R. K., Payling, R., Chenhall, B. E., Crisp, P. T., Ellis, J., and Baker, R. S. 1985. Application of x-ray photoelectron spectroscopy to the analysis of stainless-steel welding aerosols. *Applications of Surface Science* 20(4): 527–537.

14. AWS F1.2:1999, *Laboratory Method for Measuring Generation Rates and Total Fume Emission of Welding and Allied Processes*. 1999. Miami, Fla.: American Welding Society.

15. Dreon, L., Porter, K., and Wilkinson, D. 1999. Shielding gases and their effects on fume generation. *Welding Journal* 78(9): 56–58.

16. Quimby, B. J., and Ulrich, G. D. 1999. Fume formation rates in gas metal arc welding. *Welding Journal* 78(4): 142-s to 149-s.

17. *ELPI Users Manual*. Dekati Ltd. Tampere, Finland.

18. Gray, C. N., Hewitt, P., and Hicks, R. 1980. The effect of oxygen on the rate of fume formation in metal inert gas welding arcs. *Proceedings International Conference on Weld Pool Chemistry and Metallurgy* 27: 167–176. The Welding Institute.

19. Reist, P. C. 1984. *Introduction to Aerosol Science.* New York, N.Y.: Macmillan Publishing Co.

20. Hinds, W. 1999. *Aerosol Technology: Properties, Behavior, and Measurement of Airborne Particles.* Second ed. New York, N.Y.: Wiley-Interscience.

21. Casino V 2.42. 2005. Gauvin, Raynald, et al.

22. Spurny, K. R. (ed.). 1999. *Analytical Chemistry of Aerosols*. Boca Raton, Fla.: Lewis Publishers.

23. Konarski, P., Iwanejko, I., and Mierzejewska, A. 2003. SIMS depth profiling of working environment nanoparticles. *Applied Surface Science* 203: 757–761.

24. Briggs, D., and Seah, M.P. (eds.). 1983. *Practical Surface Analysis by Auger and X-Ray Photoelectron Spectroscop*y. Chichester: John Wiley & Sons.